

The Role of Replicated Service Atmosphere on Deformation and Fracture Behaviour of Carburised AISI Type 316H Steel

A.D. Warren^a, P. J. Heard^b, P.E.J. Flewitt^c and T. L. Martin^d

Interface Analysis Centre, H.H. Wills Physics Laboratory, University of Bristol,
Bristol, BS8 1FD, UK

^axander.warren@bristol.ac.uk, ^bpeter.heard@bristol.ac.uk, ^cpeter.flewitt@bristol.ac.uk,
^dtomas.martin@bristol.ac.uk

Keywords: Carburisation, Austenitic stainless steel, thermal aging, cracking, oxidation

Abstract. The UK Advanced Gas Cooled nuclear reactor fleet adopted CO₂ gas as the heat transfer medium. Over the plant service life carbon diffuses into the stainless steel components as part of the overall oxidation process. This carbon enrichment promotes carbide precipitation and changes overall microstructure, thereby altering temperature deformation and fracture behaviour. Due to difficulties of replicating the high temperature/high pressure CO₂ service environment, many tests are conducted under simulated CO₂ conditions. We compare the role of a range of surrogate atmospheres on steel test specimens to one which failed in service to establish the influence of testing atmosphere on creep deformation and fracture characteristics.

Introduction

The fleet of UK Advanced Gas Cooled Nuclear Reactor (AGR) power stations use CO₂ gas as a combined coolant and heat transfer medium [1,2]. To improve the thermal efficiency of steam generation, the AGRs were designed to operate at higher temperatures than the more widely adopted light water reactor designs [1,2]. Due to the combination of relatively high temperatures of 480–650°C (for the austenitic steel components [3]) and high pressures of CO₂ coolant, AGR boiler plant is subject to a combination of oxidation and carburisation, described by the Boudouard reaction [4]:



The service conditions result in the formation of a duplex oxide on steel components, with an outer layer of magnetite (Fe₃O₄) growing away from the initial component surface, and an inner layer of spinel (Fe_xCr_{3-x}O₄) growing inwards from the initial surface [5], Fig. 1. In this system, the bulk of the carbon generated by the Boudouard reaction diffuses into the metal, and this can be rapid along grain boundaries [5,6]. The non-equilibrium concentration of carbon alters the phase chemistry for the steel, leading to an increase in the area% of carbide precipitates [6,7]. This results in the depletion of Cr from the near surface region of the metal and results in a Cr gradient from the bulk to the surface of the metal [5,8].

It is well established that carbide precipitates formed during the fabrication of AISI Type 316H steels continue to nucleate and grow by thermal aging [9–11]. The most common carbide precipitate in AISI Type 316H steels is M₂₃C₆, where M is typically chromium, molybdenum and iron, with the ratio depending on the specific composition of the alloy [12]. Martinez-Ubeda observed M₂₃C₆ grain boundary and M₇C₃ intergranular carbides in the carburised region of an AISI Type 316H [5]. Plant assessments typically invoke data generated by tests under simulated service conditions. In many cases these tests focus on simulating load, stress state and/or temperature. Due to the difficulties in replicating AGR conditions, less attention is typically paid to atmospheric conditions – with many tests undertaken in pure CO₂ at varying pressures or in air [13]. This study compares specimens taken from tests conducted in air, pure CO₂ at atmospheric pressure and an ex-service specimen at 40 bar pressure to determine the influence of atmosphere on behaviour.

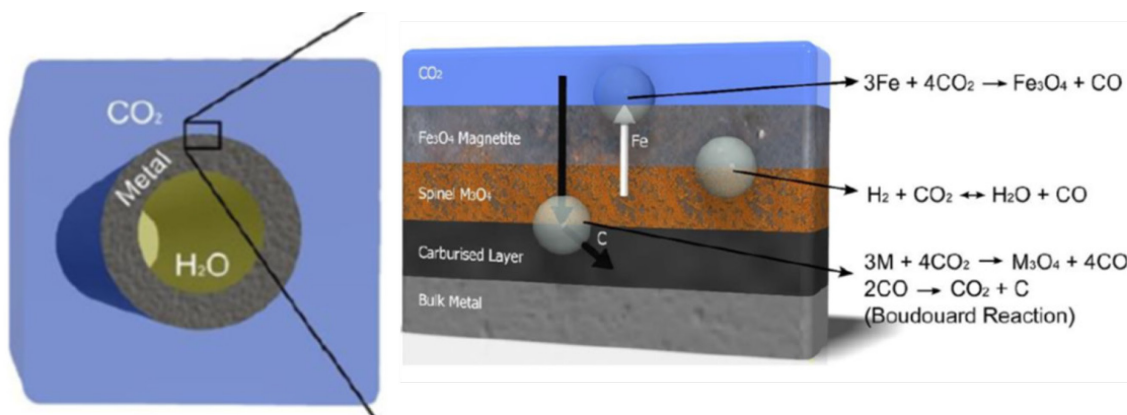


Figure 1: Schematic of surface reactions leading to oxidation and carburisation in a AISI Type 316H component in a CO_2 atmosphere, after Martinez-Ubeda [5]

Experimental

Specimen conditions and chemical compositions are detailed in table 1.

- The ex-service specimen had a complex bifurcated pipe geometry, containing two distinct regions of creep induced cracking:
 - Multiple ‘short’(>0.5 mm) cracks at the 270° location, some of which were discontinuous.
 - A continuous ‘long’ crack (~1.4 mm), in the 340° location.
- The CO_2 creep crack growth specimen exhibited different cracking behaviour at the edge of the specimen compared with the centre (the edge showed both greater crack growth, and significantly more discontinuous cracking), which may be related to the extent of CO_2 access.
- The specimen that cracked in air showed a single creep crack with limited discontinuity at the tip.

All specimens were sequentially polished for analysis using SiC papers and diamond pastes to obtain a $\frac{1}{4}\text{ }\mu\text{m}$ diamond finish, with a 0.1 colloidal silica ‘vibropolish’ finish. Scanning electron microscopy (SEM) based analyses, including energy dispersive X-ray (EDX) and electron back scatter diffraction, (EBSD), were performed on a Zeiss SIGMA VP using a Gemini FEG-SEM column, with a 30kV beam and 120 μm aperture. EBSD data were collected and processed using TSL OIM Data Collection 5 (V5.31 - EDAX Inc.) and EDX data using TEAM V4.1 (EDAX Inc.). Focused gallium ion beam analysis was performed on a FEI FIB201, with a XeF_2 “enhanced etchant” gas injector [14].

Table 1: Specimen exposure conditions and compositions

Specimen ID	Test conditions										
	Temperature (°C)	Load		Duration (hrs)	Crack growth rate (mm/hr)	Atmosphere					
Ex-service	505	Complex multi-axial			145,000	Unknown		600 psi: bulk CO_2 with additions of CO , H_2 , H_2O & CH_4			
CO_2 Exposed	525°C	Load increased from $K=23.5\text{ MPa.m}^{0.5}$ to $K=33\text{ MPa.m}^{0.5}$ at 32,49hr			48,614	7.2×10^{-3}		Atmospheric pressure CO_2			
Air	525	Load increased from $K=23.5\text{ MPa.m}^{0.5}$ to $K=33\text{ MPa.m}^{0.5}$ after 32kh			48,000	3.6×10^{-3}		Air			
Specimen	Composition (wt%)										
	C	S	Si	Mn	P	Cr	Mo	Ni	Co	Cu	B
Ex-service	0.06	0.005	0.63	1.78	0.035	16.55	2.35	14.12	0.024	0.046	-
CO_2 & Air tests	0.055	0.014	0.32	1.45	0.021	17.18	2.32	10.92	0.08	-	0.003

Results and Discussion

Service Exposed. The surface of the ex-service specimen showed a duplex (magnetite/spinel) oxide with a thickness of 20 to 60 μm . The specimen exhibited surface carburisation extending to a depth of $\sim 100 \mu\text{m}$. Sporadic spinel oxide intrusions were observed within the carburised layer. Carbide precipitates in the carburised layer were continuous along grain boundaries. The latter had a range of 0.28 to 1.86 μm , whilst in the bulk precipitates were discontinuous with sizes in the range 0.25 to 0.82 μm . The long creep crack at the 340° location in the ex-service specimen contained regions of duplex oxide extending from the crack tip, Fig. 2. The grain boundaries ahead of the crack were enriched in Cr by ~ 3 wt%; this extended for $\sim 50 \mu\text{m}$ from the crack. Grain boundaries at a similar depth in the bulk of the specimen showed no corresponding elemental enrichment. The carbide structure was revealed using the FIB-XeF₂ etching technique [14], Fig. 3. Carbides in the first $\sim 40 \mu\text{m}$ of grain boundary ranged from 0.25 to 2.17 μm (mean 0.79 μm) - a significant increase compared to the bulk material; these carbides were discontinuous. The shorter cracks at the 270° location also have a duplex magnetite-spinel oxide extending from crack tips. EDX microanalysis of the regions ahead of the leading discontinuous crack, figure 4, shows no Cr enrichment. The carbide precipitation was continuous along grain boundaries immediately ahead of the crack, in a size range of 0.24 to 1.69 μm (mean 0.51 μm). Both cracked regions in the ex-service specimen show evidence of carburisation at the crack tip, which is more extensive in the larger crack.

CO₂ Exposed. The CO₂ gas exposed material had a thin, uneven, duplex surface oxide of 5 to 25 μm thickness. The carbide precipitate distribution in the bulk of these specimens is highly variable, ranging from 0.12 to 1.32 μm (mean 0.36 μm) maximum extension, Fig. 4. No significant difference was observed in the carbide size distribution between the specimens retrieved from the centre of the creep cracked test specimen compared with close to the edge. The centre crack shows duplex oxide to the tips, albeit with significantly less fill than in the ex-service specimen. Given the shorter duration exposure, this is not unexpected. EDX composition mapping revealed no elemental enrichment at grain boundaries ahead of the crack tip, Fig. 5a. FIB-XeF₂ imaging shows carbide precipitates ahead of the crack tip in the size range 0.12 to 1.30 μm (mean 0.43 μm). Whilst this corresponds to a small increase in mean size, all the carbide precipitates measured within the first $\sim 40 \mu\text{m}$ of grain boundary are within the expected distribution for the bulk material. The edge crack again has a duplex oxide, but as with the central crack, there is less oxide fill than the ex-service specimens. Again, no elemental enrichment was detected ahead of the crack tip using EDX. The carbide precipitate size distribution was 0.12 to 1.42 μm (mean 0.41 μm). The mean is consistent with that from the central crack, although the edge also features an increased maximum carbide precipitate size. However, the precipitates responsible for this increase lie almost 40 μm away from the crack tip. Based on the EDX and FIB-XeF₂ results, atmospheric pressure CO₂ does not cause crack-tip carburisation, and there are no microstructural indicators for the difference in cracking behaviour between the edge and centre of the specimen.

Air exposed. The air exposed specimen showed a surface duplex oxide 120 to 150 μm thick. The crack was less oxide filled than either the ex-service or the CO₂ exposed specimens, whilst still exhibiting elongated nodules of duplex oxide. EDX composition microanalysis showed no Cr enrichment ahead of the crack tip, Fig. 6a, although the crack was found to intersect a MnS inclusion, which appears to have oxidised. A carbide precipitate size range of 0.09 to 0.46 μm (mean 0.22 μm) was measured in the bulk, and 0.09-0.69 μm (mean 0.20 μm) ahead of the crack, Fig. 6b.

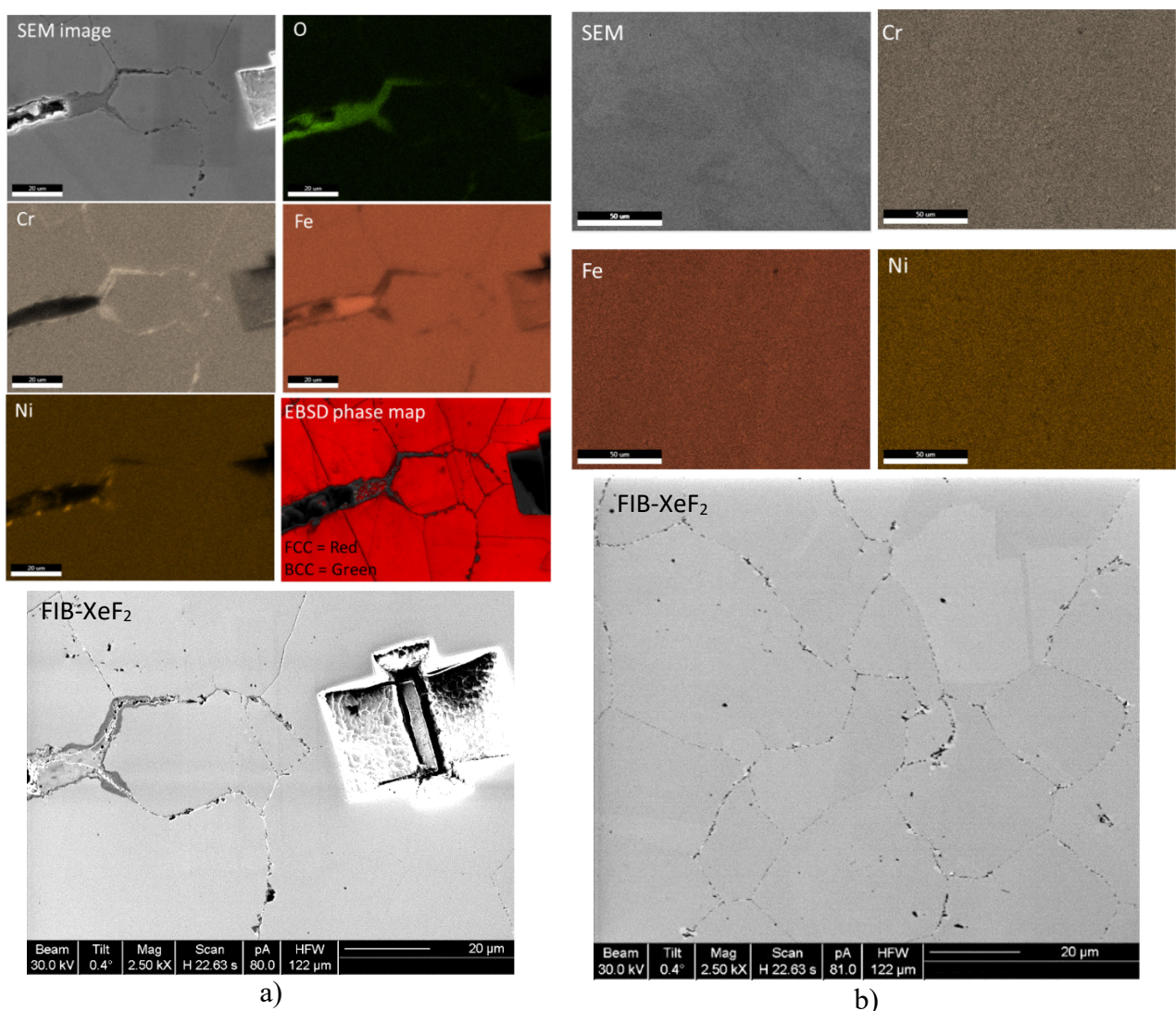


Figure 2: SEM/EDX/EBSD/FIB-XeF₂ analysis of crack tip at 340° location in ex-service specimen,
a), compared to bulk material at a comparable depth,
b). Carbide precipitates appear as dark grey in FIB-XeF₂ images

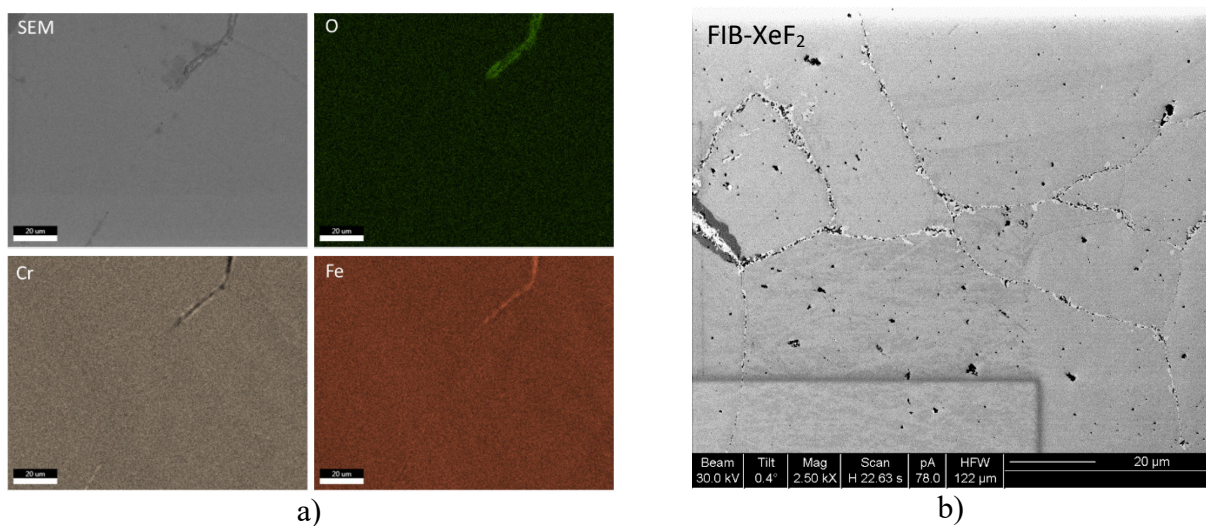


Figure 3: SEM/EDX/FIB-XeF₂ analysis of crack tip at 270° location in ex-service specimen,
a) EDX analysis and b) FIB-XeF₂

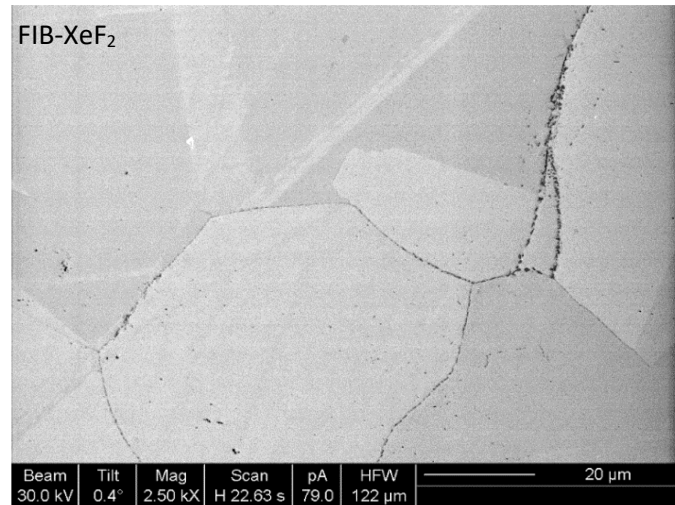


Figure 4: FIB-XeF₂ image of carbide precipitates in the bulk of the CO₂ exposed specimen

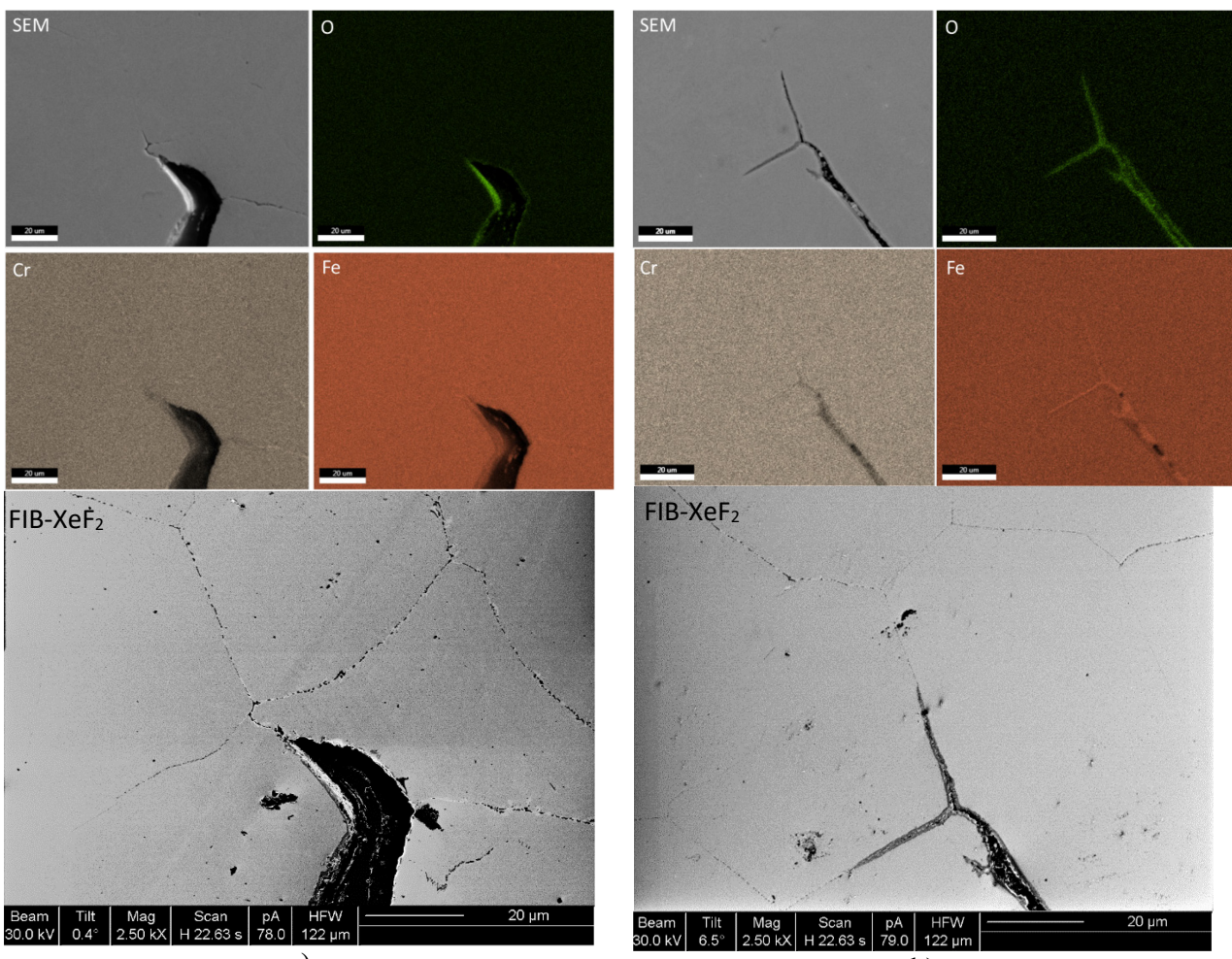


Figure 5: EDX/FIB-XeF₂ analysis of CO₂ exposed specimens. a) centre and b) edge

Concluding Comments

The regions directly ahead of the crack tips in the ex-service specimen were found to show both increased carbide precipitate size, and in the case of the long crack, grain boundary Cr enrichment. Hence carburisation occurs during creep induced cracking, with the more extensive crack giving better gas access. Surrogate test conditions (atmospheric pressure air and atmospheric pressure CO₂) do not replicate this behaviour, so the suitability of the experimental surrogates must be reassessed.

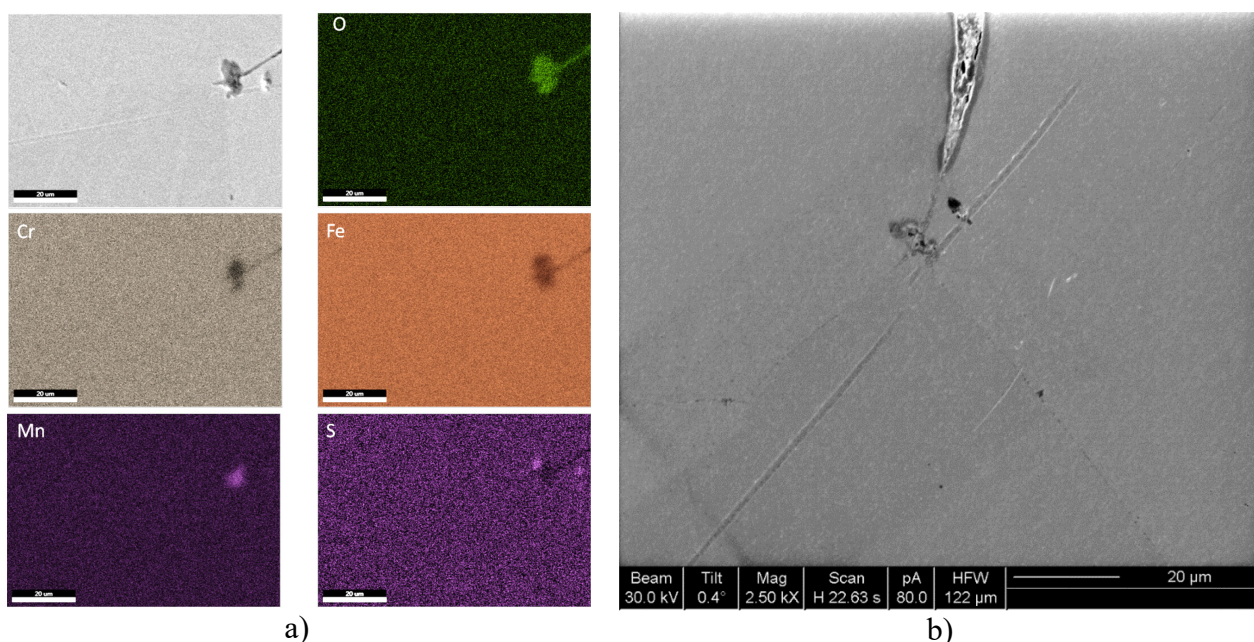


Figure 6: EDX/FIB-XeF₂ analysis of air exposed specimen, a) EDX analysis and b) FIB-XeF₂

Acknowledgements

The authors acknowledge financial support by EDF Energy Ltd. and Innovate UK (ENCAMP) and EDF Energy for provision of materials.

References

- [1] J. W. Taylor: AGR Boiler Materials Selection considerations, in: *Gas-Cooled React. Today*, British Nuclear energy Society, Bristol, UK (1982) p.328
- [2] G. B. Gibbs & L. A. Popple: Nucl. Energy Vol. 21 (1982) p. 51-55
- [3] A.I. Martinez-Ubeda et al.: Key Eng. Mat. Vol.713 (2016) p. 1-4
- [4] F. Rouillard et al.: Oxid. Met. Vol 77 (2012) p. 57-70
- [5] A. I. Martinez-Ubeda: 2017, Effect of composition variation and service environment on the long term ageing of Type 316H austenitic stainless steels, PhD thesis, University of Bristol
- [6] H. J. Grabke & I. Wolf: Mater. Sci. Eng. Vol. 87 (1987) p. 23–33
- [7] N. Birks et al.: ‘*Introduction to the high temperature oxidation of metals*,’ Cambridge University Press, UK 2006
- [8] C. Ostwald & H. J. Grabke: Corros. Sci. Vol. 46 (2004) p. 1113–1127
- [9] B. Weiss & R. Stickler: Met. Trans. Vol.3 (1972) p. 851–866
- [10] A. F. Padilha & P. R. Rios: ISIJ International Vol. 42 (2002) p. 325–337
- [11] L. P. Stoter: J. Mat. Sci Vol. 16 (1981) p. 1039–1051
- [12] W. E. White & I. Le May: Metallography Vol. 3 (1970) p. 51–60
- [13] B. Chen; 2011, Effects of thermo–mechanical history on creep damage in 316H austenitic steel, PhD thesis, University of Bristol
- [14] C. Liu, P. J. Heard, O. D. Payton, L. Picco and P. E. J. Flewitt: submitted to Ultramicroscopy (2018)